PROCEEDINGS OF ECOS 2026 - THE 39TH INTERNATIONAL CONFERENCE ON

EFFICIENCY, COST, OPTIMIZATION, SIMULATION AND ENVIRONMENTAL IMPACT OF ENERGY SYSTEMS

28 JUNE – 03 JULY, 2026, CONSTANTA, ROMANIA

Heat exchanger design model for ammonia preheating and evaporation for cracking process

Chiara Monacchini[a], Daria Bellotti[b], Alessandro Sorce[c]

[a]*Thermochemical Power Group (TPG), University of Genoa,Genoa, Italy chiara.monacchini@edu.unige.it CA*
[b]Thermochemical Power Group (TPG), University of Genoa, Genoa, Italy daria.bellotti@.unige.it
[c]Thermochemical Power Group (TPG), University of Genoa, Genoa, Italy alessandro.sorce@unige.it

Abstract

The urgent need to reduce carbon emissions is driving the development of alternative and low-carbon fuels. In recent years, ammonia has gained increasing attention as a fuel for power generation due to its favourable chemical properties. Additionally, ammonia serves as an effective hydrogen carrier, supported by a well-established production process based on the Haber–Bosch method. Compared to pure hydrogen, ammonia offers advantages in terms of storage and transportation, as it can be stored and handled in liquid form at moderately low pressures and temperatures. Thanks to these characteristics, ammonia can be efficiently delivered to power generation sites and subsequently decomposed into hydrogen and nitrogen through a cracking process carried out directly on-site. However, to supply ammonia to the reactor, it must be brought from liquid storage conditions to gaseous conditions. This requires a dedicated thermal system capable of ensuring both complete evaporation and sufficient heating up to the operating conditions required for the cracking process. For this reason, a heat exchanger model was developed and analysed to enable the heating and evaporation of ammonia up to the target cracking conditions. This work focuses on the development of a MATLAB-based calculation code for the design and analysis of a once-through finned-tube heat exchanger dedicated to heating and evaporation of ammonia before the cracking process. The developed program integrates thermodynamic and heat transfer models to simulate and evaluate different system configurations, allowing for the variation of both geometric parameters and operating conditions. The objective is to identify a heat exchanger design capable of efficiently heating ammonia to the optimal conditions required for ammonia decomposition. Based on this configuration, further analyses have been conducted to investigate the behaviour of heat exchangers under off-design conditions.

Keywords:

Alternative Fuel; Ammonia; Cracking Process; Gas Turbine; Heat Exchanger.

1. Introduction

Nowadays, one of the key issues in the energy sector is research on the transition from fossil fuels to alternative energy sources, aimed at achieving decarbonization. The goal is therefore to reduce greenhouse gas emissions (GHG), among which carbon dioxide (CO_2) is by far the largest contributor to GHG emissions over time [1]. One strategy is to employ energy systems that do not rely on fossil fuels, as widely recognised renewable sources. However, due to their inherently intermittent nature, driven by seasonal, climatic, and atmospheric variations, they cannot always match the grid's electricity demand in real time. In this framework, chemical compounds, owing to their high energy density and ease of storage, transport, and distribution, represent a promising option for large-scale energy storage [2]. Among these, hydrogen (H_2) has emerged over the past decades as a particularly significant energy carrier, as it does not produce CO_2 emissions during combustion and has a high energy content per unit mass [3]. Unfortunately, with today's technologies, building an energy economy based entirely on pure hydrogen still presents substantial technical and economic challenges. One of the main obstacles is hydrogen storage and transportation, which requires highly specialised and expensive equipment [4]. To store hydrogen in liquid form, it must be cooled and continuously maintained at temperatures below −253 °C, at atmospheric pressure, demanding high energy consumption, complex insulation systems, and strict safety measures, all of which increase costs and limit large-scale deployment. Alternatively, hydrogen can be stored in its gaseous form; however, due to its extremely low volumetric energy density, this approach requires compression to extremely high pressures (up to 700 bar). As a result, despite hydrogen's attractive characteristics as a clean energy carrier, its storage and handling

remain major barriers to the widespread adoption and have driven growing interest in alternative hydrogen carriers. Among these, ammonia stands out as a promising carbon-free energy carrier and hydrogen storage medium, in addition to its long-standing role as a fertiliser [5]. Due to its ease of large-scale production using well-established industrial processes such as the Haber-Bosch method, along with mature handling and distribution infrastructure and high hydrogen content (17.6% by weight), ammonia has further strengthened its position as a hydrogen carrier [5]. Moreover, it can be liquefied under relatively mild conditions, around 10 bar at room temperature or -33 °C at atmospheric pressure, making its storage and transportation considerably easier and cost-effective than those of hydrogen [6]. In fact, ammonia can be stored in liquid form with a higher volumetric energy density than liquid hydrogen (15.6 MJ/l for NH_3 compared to 9.1 MJ/l for H_2) [7]. The cost of transporting ammonia is orders of magnitude lower than that of transporting hydrogen [8]. Additionally, it can be cracked into hydrogen at the point of use for fuel cells, gas turbines and other hydrogen-based technologies. Ammonia decomposition represents an effective pathway for carbon-free hydrogen production, as it produces only nitrogen and hydrogen as final products. Ammonia cracking is an endothermic reaction that requires the input of thermal energy to dissociate stable NH_3 molecules into H_2 and N_2. In the absence of a catalyst, efficient decomposition occurs only at high temperatures, above 670 °C, and even higher temperatures when the operating pressure rises (800-900°C). However, the use of suitable catalysts allows the reaction temperature to be significantly reduced, enabling substantial NH_3 conversion at temperatures below 600 °C [9]. Thermodynamic analysis based on Gibbs free energy minimisation indicates that NH_3 decomposition is strongly temperature-dependent between 250 and 450 °C, whereas further increases in temperature above 450 °C do not lead to significant improvements in conversion [10]. Owing to the equilibrium nature of the reaction, high temperatures are thermodynamically favourable for achieving high conversion levels. Consequently, starting from a liquid storage state, it is necessary to achieve the high-temperature gaseous conditions needed by the cracking process. This requires the use of a dedicated thermal conditioning unit capable of ensuring both evaporation and heating of the stream. In our work, this process is achieved by exploiting the thermal energy contained in the exhaust gases of a turbine. This heat, which would otherwise be wasted as residual or waste heat, is recovered and reused to supply the energy needed for evaporation and heating phases [11], [12], [13].

The present study aims to develop a model of the thermal unit, as mentioned above, responsible for transferring ammonia from a liquid state to a high-temperature gaseous phase, required for the subsequent decomposition phase in a dedicated reactor. To this end, a dedicated MATLAB-based model has been developed, enabling the analysis of heat exchange conditions within the system. This method enables a more accurate characterisation of the unit's thermal behaviour and constitutes a useful tool for analysing its operating behaviour under different conditions. Furthermore, this approach can be applied to any other facility where it is appropriate to utilise the waste heat from exhaust gases. Given the novelty of the proposed system, no experimental datasets are currently available in the literature, to the best of the authors' knowledge. Therefore, a direct validation against experimental data could not be performed at this stage. Nevertheless, the reliability of the obtained results is assessed by comparing the calculated values with typical ranges reported in the literature, proving to be physically consistent and credible. Moreover, additional consistency checks are carried out using commercial software based on well-established heat exchanger models showed relative errors between 2% and 6%.

2. Materials and methods

This study investigates the design and operational behaviour of the thermal unit positioned upstream of the cracking reactor. The unit is composed of three parts: a preheater (economiser), which increases the temperature of liquid ammonia to reach saturation conditions before evaporation; an evaporator, where the phase change from liquid to gaseous ammonia takes place; and a superheater, which further elevates the temperature of the ammonia gas to the reactor's operating conditions. The entire process is driven by the recovery and efficient utilisation of heat from the exhaust gases [14]. The gas stream enters the reactor, where it undergoes a decomposition reaction; since this reaction is endothermic, an external heat source will be required. After the cracking reaction, hydrogen is separated from the gas mixture and used in the gas turbine for energy generation. In order to reduce system complexity and limit the required design modifications, hydrogen is considered as the fuel, since the combustion chamber is already designed to operate with it and can therefore be used without significant changes. This approach avoids the need to redesign the combustion chamber to handle an ammonia fuel mixture, which would involve additional technical challenges and development work.

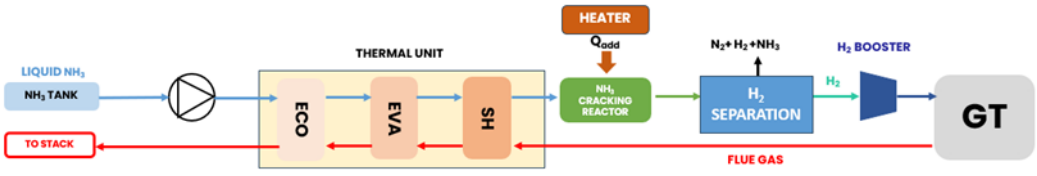

Figure 1. *Layout scheme [14].*

The calculation framework has been developed in the MATLAB environment, exploiting REFPROP software program for the determination of thermophysical properties of fluids. The thermal unit design considered in this study is a once-through configuration, motivated by its compactness [15], as this design allows a significant reduction in overall system size due to the complete absence of steam drums, unlike conventional Heat Recovery Steam Generators (HRSG) employed in combined-cycle gas turbine plants. However, this configuration does not allow for a clear geometrical separation between the three main sections of the system, namely the economiser, evaporator, and superheater. Consequently, the transition points between the economiser and the evaporator, as well as between the evaporator and the superheater, corresponding to the phase change from single-phase to two-phase flow and vice versa, are not fixed but vary depending on the conditions under examination. For this reason, these sections represent the most complex components to model and are also the most relevant from a thermophysical standpoint. In the following sections, the calculation methodology of each part will be described in detail.

2.1 Pre-heating section

Starting from the geometry and both fluids' inlet conditions, the calculation system is based on the ε−NTU method [16]. The determination of the Number of Transfer Units (NTU) requires the evaluation of the overall heat transfer coefficient. Consequently, the first step of the analysis consists of estimating the equivalent thermal resistance U, which accounts for all the thermal resistances of the system between the inner and outer fluids, including internal convection, conduction through the pipe wall, and external convection [15]. This evaluation must also account for the fin efficiency (η_T).

For the calculation of the convective heat transfer coefficient of the cooling gas h_{GAS}, the approach is based on the use of a dimensionless number that relates the Nusselt, Reynolds, and Prandtl numbers, namely the Stanton number (St), defined as:

$$St = \frac{Nu}{Re\,Pr}, \qquad (1)$$

Introducing the Colburn factor definition [17]:

$$j = St\,Pr^{2/3} \quad 0.6 < Pr < 60 \qquad (2)$$

and substituting the definition of the Nusselt number, an explicit expression for the gas-side convective heat transfer coefficient is finally obtained:

$$h_{GAS} = j\,\frac{k_{GAS}}{d_o}\,Re_{GAS}\,\mathrm{Pr}_{GAS}^{1/3}, \qquad (3)$$

where k_{GAS} is the gas thermal conductivity and d_o is the outside tube diameter.

For the ammonia side, having a single-phase liquid, it is possible to use the Dittus-Boelter correlation:

$$h_{NH_3} = 0.023\,\frac{k_{NH_3}}{d_i}\,Re_{NH_3}^{0.8}\,\mathrm{Pr}_{NH_3}^{0.4}, \quad (4)$$

Finally, the overall heat transfer coefficient U and then NTU can be calculated as follows:

$$U = \frac{1}{\left[\frac{1}{h_{NH3}} + \left(\frac{A_{ip}}{(2\pi\,k_w N_{tr})L}\right)\cdot ln\left(\frac{d_o}{d_i}\right) + \left(\frac{A_{ip}}{A_{op}}\right)\cdot\frac{1}{\eta_t h_{GAS}}\right]} \qquad (5)$$

$$NTU = A_{ip}\cdot\frac{U}{C_{min}} \qquad (6)$$

where C_{min} is the minimum heat capacity rate, A_{ip} is the inside heat transfer area per pass, A_{op} outside heat transfer area per pass and η_t is the fin efficiency.

An average pass effectiveness can be estimated considering the expression for a cross-flow heat exchanger with both fluids unmixed [17]:

$$\varepsilon_p = 1 - exp\left(\frac{exp\left(-r\,NTU^{0.78}\right)-1}{r\,NTU^{-0.22}}\right), \quad (7)$$

Where r is the ratio between the minimum and maximum heat capacity rate.

From the previous equation, an overall effectiveness is calculated [15]:

$$\varepsilon_{oa} = \frac{\left(\frac{1-\varepsilon_p\,r}{1-\varepsilon_{p,ECO}}\right)^n - 1}{\left(\frac{1-\varepsilon_p\,r}{1-\varepsilon_p}\right)^n - r}, \qquad (8)$$

where n is the number of passes required in the economiser section.

From $\varepsilon_{p,ECO}$ definition, the gas temperature is determined:

$$T_{GAS,i} = \frac{r\,\varepsilon_{oa}\,T_{NH_3,i} - T_{GAS,o}}{r\,\varepsilon_{oa} - 1} \qquad (9)$$

Based on the energy balance, the ammonia enthalpy can be calculated, and consequently its temperature:

$$h = h_{in} + \frac{Q}{m_{NH3}} \qquad (10)$$

This is an iterative procedure that continues up to the saturation temperature; however, the calculation must be stopped before the onset of the phase change [18]. The heat transfer area required to complete the attainment of the saturation temperature is therefore assessed. In the subsequent section, the evaporation process begins, which requires a different modelling approach, as the working fluid becomes two-phase.

2.2 Evaporating section

The scheme of the evaporation section is still based on the ε-NTU method; in particular, on the gas side, there are no particular differences compared to previous cases. On the contrary, for the ammonia side, the procedure becomes more complex because it is necessary to refer to an appropriate system capable of calculating the heat transfer coefficient for the two-phase fluid. To do this, the Kandlikar correlation is employed [19], [20] :

$$\frac{h_{NH_3(tp)}}{h_{NH_3(L)}} = C_1 Co^{C_2} (25\ Fr_L)^{C_5} + C_3 Bo^{C_4} F_{fl} \quad , \qquad (11)$$

where $h_{NH_3,EVA\,(tp)}$ is the two-phases heat transfer coefficient during the vaporization process, $h_{NH_3,EVA\,(L)}$ is the single-phase heat transfer coefficient for the entire flow as liquid flow, Co is the convection number, Bo is the nucleate Boiling number , Fr_L is the Froude number and F_{fl} is a fluid-surface parameters which should be taken as 1.0 for stainless tubes [16]. The definitions of the parameters aforementioned are provided below:

$$Co = \left(\frac{1-x_{av}}{x_{av}}\right)^{0,8} \left(\frac{\rho_{NH_3,V}}{\rho_{NH_3,L}}\right)^{0,5}, \qquad (12)$$

$$Bo = \frac{Q''}{G_{NH_3} h_{fg}}\ , \qquad (13)$$

$$Fr_L = \frac{G_{NH_3}^2}{\rho_{NH_3,L}^2\, g\, d_{i,EVA}} \qquad (14)$$

where G_{NH3} is the mass flux $(\frac{kg}{s\ m^2})$, Q'' is the heat flux $\left(\frac{W}{m^2}\right)$, and h_{fg} is the latent heat of vaporisation.

The constants $C_1, C_2, C_3, C_4,$ and C_5 are reported in Table 1, as a function of the boiling region:

Table 1. *Constant values for Kandlikar correlation [20].*

	Convective Boiling	Nucleate Boiling
C_1	1.1360	0.6683
C_2	-0.9	-0.2
C_3	667.2	1058.0
C_4	0.7	0.7
C_5	0.3	0.3

The choice of the values is based on the convection number Co, as shown in Table 2:

Table 2. *Definition of the boiling region as a function of Co.*

	Boiling Region
$Co < 0.65$	Convective
$Co > 0.65$	Nucleate

In the convective region, the predominant heat transfer mechanism is convection, while in the nucleate boiling region, the predominant mechanism is nucleate boiling. A revised overall heat transfer coefficient U is calculated, as described above. Then a new pass effectiveness can be evaluated using a modified effectiveness formulation, since the heat capacity ratio is zero because the ammonia evaporates at nearly constant temperature, resulting in a very large c_p:

$$\varepsilon = 1 - exp^{(-NTU)} \qquad (15)$$

At this point, an iterative calculation procedure is carried out to determine the heat transfer area required to complete the evaporation process. The iterative loop is terminated when the vapour quality reaches unity. Since the system operates in a once-through configuration, as previously discussed, the evaporation process is completed in a pass; however, the beginning of superheating already occurs within the same pass.

2.3 Superheating section

For this section of the system, it is unnecessary to describe the program structure in detail, as it is similar to that of the economiser (paragraph 2.1). In both cases, the working fluids return to a single-phase condition;

the only difference is that, in this case, both fluids are in the gaseous phase. The only substantial distinction concerns the control criterion used to exit the iterative loop and, consequently, the determination of the number of superheater passes. Unlike the economiser, the exit condition of the iterative cycle is no longer based on the ammonia temperature, but on the inlet temperature of the gas. The number of superheater passes can be determined by simply counting the sections of the system in which the inlet temperature is lower than the actual exhaust gas temperature. In general, the calculated temperature is lower than the value specified in the initial conditions. This occurs because the superheater ends with the last complete pass for which the entering gas temperature is less than or equal to the originally specified gas inlet temperature. Inherently, this result is unsatisfactory, since the inlet gas temperature is an independent variable determined by the gas turbine power setting. To achieve a match, the gas outlet temperature is incrementally increased [15]. Each time the outlet temperature is raised, the entire waste heat recovery unit calculation is repeated, and the resulting superheater gas inlet temperature is compared with the gas turbine exhaust temperature. Once the two temperatures are aligned, a minimum acceptable convergence threshold is therefore established, typically in the range of 0.1-0.5 °C, and the design is finalised.

2.4 Pressure drops calculation

As the final step of the methodology, the pressure drop is evaluated for the three sections of the unit. In this preliminary analysis, concentrated pressure losses have been neglected as a first approximation. The calculation methods for the two working fluids are outlined below.

The pressure drop on the gas side is calculated using the following correlation, which relates frictional losses to the fluid properties, flow conditions, and geometric characteristics [15]:

$$\Delta p_{GAS} = \frac{\left(2\, f_{D,GAS}\, G_{GAS}^2 N_{tr}\right)}{\rho_{m,GAS}}, \qquad (16)$$

Where f is the Darcy coefficient, and G is the mass flow per unit of area.

For ammonia pressure drop calculation (single-phase), since the fluid is single-phase and flows inside tubes, the Darcy–Weisbach equation is used [16]:

$$\Delta p_{NH_3} = f_{D,NH_3}\, \frac{L_1}{d_i}\, \frac{\rho_{m,NH_3}\, v_{m,NH_3}^2}{2}, \qquad (17)$$

The Darcy friction factor is calculated using the Petukhov correlation [17]:

$$f_{D,NH_3} = (0.79\, \ln(Re) - 1.64)^{-2} \qquad 3000 < Re < 5 \cdot 10^6 \qquad (18)$$

Unlike the economiser case, where the fluid is single-phase, in the evaporator, ammonia exists in both liquid and vapor phases, making the pressure drop calculation considerably more complex. For ammonia, a specific correlation has been adopted to describe the vaporisation process, allowing for proper accounting of the two-phase flow behaviour. Among the available correlations, the Lockhart–Martinelli method was chosen, as used in reference [21]. This correlation, based on the separated flow model, treats liquid and vapor as two distinct fluids. The two-phase pressure drop is given by:

$$\Delta p_{tp,NH_3} = \Phi_L^2 \Delta p_L, \qquad (19)$$

$$\Delta p_{tp,NH_3} = \Phi_G^2 \Delta p_G, \qquad (20)$$

Where the single-phase pressure drops are:

$$\Delta p_{L,NH_3} = \frac{2 f_{L,NH_3} G_{NH_3}^2 \left(1 - x_{av-NH_3}\right)^2}{\rho_{L,NH_3} d_i}, \qquad (21)$$

$$\Delta p_{G,NH_3} = \frac{2 f_{G,NH_3} G_{NH_3}^2\, x_{av-NH_3}^2}{\rho_{G,NH_3} d_{i-EVA}}, \qquad (22)$$

f_L and f_D are single-phase liquid and gas friction factor respectively, calculated as follows:

$$f_{L,NH_3} = \frac{0.079}{Re_{L,NH_3}^{0,25}} \quad Re_{L,NH_3} = \frac{G_{NH_3}\left(1 - x_{av,NH_3}\right) d_i}{\mu_L} \qquad (23)$$

$$f_{G,NH_3} = \frac{0.079}{Re_{G,NH_3}^{0,25}} \quad Re_{G,NH_3} = \frac{G_{NH_3}\, x_{av-NH_3} d_i}{\mu_G} \qquad (24)$$

Multiplicative coefficients Φ_L^2 and Φ_G^2 are calculated using Chisholm's relations [21]:

$$\Phi_L^2 = 1 + \frac{C}{X} + \frac{1}{X^2}, \qquad (25)$$

$$\Phi_G^2 = 1 + CX + X^2, \qquad (26)$$

where X is the Martinelli parameter and constant C is a tabulated coefficient depending on the flow regime:

$$X = \sqrt{\frac{\Delta p_{L-NH_3}}{\Delta p_{G-NH_3}}}, \qquad (27)$$

Table 3. *Value of C for Lockhart Martinelli model [21].*

Liquid Phase	Gas Phase	C
Turbulent	Turbulent	20
Viscous	Turbulent	12
Turbulent	Viscous	10
Viscous	Viscous	5

3. System description

The thermal unit is designed to gradually heat the ammonia, allowing it to change phase from liquid to vapour while efficiently bringing it to the high temperatures needed for the next stage of the cracking process. This is accomplished through a once-through configuration, recovering heat from the gas turbine exhaust. The geometry of the thermal unit has been chosen after reviewing several studies on such systems, leading to the conclusion to adopt a cross-flow finned tube exchanger with segmented fins [16], [17]. The selected configuration adopts finned tubes in order to enhance heat transfer (Figure 2). This geometry allows for an increase in heat exchange, causing, on the other hand, a slight increase in pressure drop on the external fluid side. In this model, it has been considered to partition ammonia mass flow into several pipes with a smaller diameter to enhance the thermal mechanism.

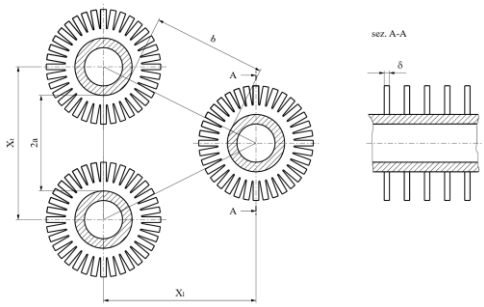

Figure 2. *Segmented finned-tube arrangement [16]*

The operating conditions of the system under investigation are reported in Table 4. These parameters characterise both the heat source and the heat sink involved in the thermal integration process. On the exhaust gas side, the inlet temperature to the system $T_{\mathrm{GAS,in}}$ is known, together with the operating pressure and the exhaust gas mass flow rate $\dot{m}_{\mathrm{GAS}}$. These variables describe the thermal potential available from the exhaust stream for heat recovery. On the ammonia side, the storage temperature $T_{\mathrm{NH_3,in}}$ is specified, the working pressure and the nominal ammonia mass flow rate $\dot{m}_{\mathrm{NH_3}}$ are also defined, as they determine the operating conditions and the thermal demand of the ammonia heating and vaporising process.

Table 4. *Input data.*

Parameter	Value
Gas Side	
$\mathrm{T_{GAS,in}}$	$445.50\ °\mathrm{C}$
$\mathrm{p_{GAS}}$	$1.0125\ \mathrm{bar}$
$\dot{\mathrm{m}}_{\mathrm{GAS}}$	$55.49\ \mathrm{kg/s}$
Ammonia side	
$\mathrm{T_{NH_3,in}}$	$-33\ °\mathrm{C}$
$\mathrm{p_{NH_3}}$	$45\ \mathrm{bar}$
$\dot{\mathrm{m}}_{\mathrm{NH_3}}$	$2.26\ \mathrm{kg/s}$

The final preliminary datum concerns the material used for the manufacture of the tubes and fins, which must be selected with particular attention to the fluid ammonia, as it is especially corrosive. Consequently, the material must be capable of effectively withstanding this chemical aggressiveness. It is highlighted that in the liquid phase, ammonia is compatible with AISI 316 steel, an austenitic stainless steel, which ensures adequate corrosion resistance and operational reliability. For the subsequent stages, in which ammonia is no longer solely in the liquid phase, it was therefore considered, as a first approximation, to adopt this stainless steel for all components, ensuring consistency in material selection and adequate corrosion resistance throughout the entire system [22].

4. Results

As a first step in the procedure, the front dimensions of the heat exchanger have been determined, which are essential for calculating the number of tubes and, consequently, the ammonia flow rate per tube. In particular, a range of factors has been taken into account, including the space required at the turbine outlet. In addition, particular attention has been given to avoiding excessively high gas velocities at the inlet of the unit, which could arise in the case of an excessively small frontal area, as shown in the map in Figure 3.

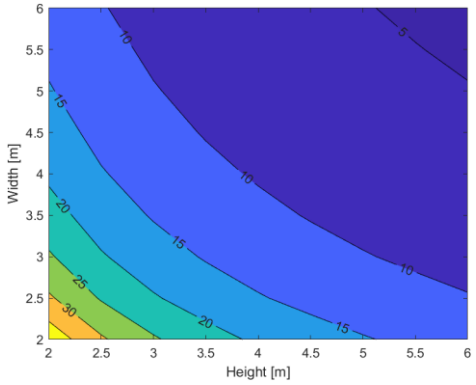

Figure 3. *Gas speed as a function of frontal area dimensions.*

Following a preliminary assessment based on the gas turbine layout, a configuration with a frontal area of 6 m in length and 3 m in height has been selected; the overall external diameter of the tubes, including fins, is 40 mm. The fins are characterised by a thickness of 1 mm, and 200 fins per meter are considered. Furthermore, an increase in diameter has been introduced for the evaporation and superheating phases. This has been done to achieve speeds that improve heat exchange performance without causing significant pressure losses. Geometrical data have been reported in Table 5.

Table 5. *Main geometrical data.*

Length	Height	$d_{i\text{-}ECO}$	$d_{i\text{-}EVA/SH}$	d_e	N_{tr}
m	m	mm	mm	mm	
6	3	10	25	40	60

Based on this geometry, a required number of 60 tubes per row has been calculated, with a thickness of 5 mm, which means a mass flow rate per individual tube of 0.038 kg/s. The methodology outlined in the previous section has been applied to the present case study. The resulting configuration comprises 8 passes, with a total tube length of 48 m and a total depth of 400 mm. The superheating section occupies the majority of this length, as this is where the largest temperature difference occurs, starting from the saturation temperature. Under these conditions, the outlet temperature of the ammonia is high, around 437 °C, with a little temperature difference at the approach point of 9 K, but the gas side is also quite high, around 353°C (Figure 4). This heat, equal to 21 MW, could be harnessed for further recovery.

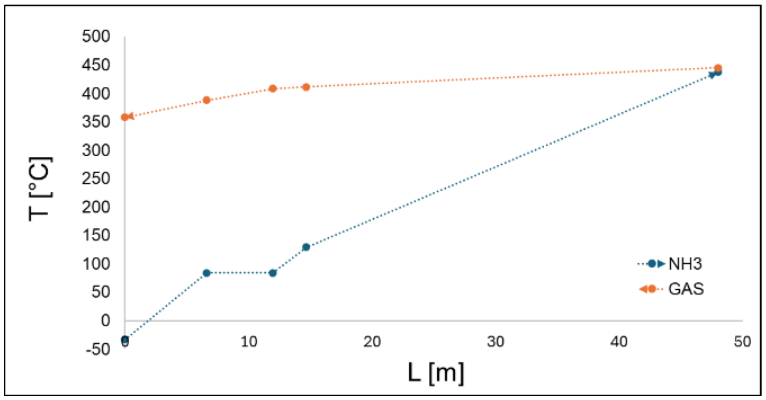

Figure 4. *Ammonia and gas temperatures along the length of the tubes.*

One essential parameter is the heat transfer coefficient (*h*), in this case, the values on the two sides are significantly different, more than one order of magnitude, with the gas-side coefficient being much lower than

the ammonia-side coefficient, as reported in Table 6. This difference arises because gas has lower density and thermal conductivity. As a result, convective heat transfer on the gas side is less effective, despite the adoption of serrated fins, leading to a lower heat transfer coefficient compared to the ammonia side, and the overall heat transfer is mainly limited by the gas-side resistance. Analysis of thermal resistances shows that the dominant contribution comes from convection on the finned side, while heat conduction through the metal wall is almost negligible. The addition of fins significantly increases the effective heat transfer area, reducing convective resistance and increasing the overall U-value.

Table 6. *Heat transfer coefficients of gas and ammonia sides.*

	h_{GAS}	h_{NH_3}	R_{cond}	$R_{conv,GAS}$	U
	$\frac{W}{m^2K}$	$\frac{W}{m^2K}$	$\frac{m^2K}{W}$	$\frac{m^2K}{W}$	$\frac{W}{m^2K}$
ECO	31.55	5450.02	$1.2 \cdot 10^{-4}$	$2.7 \cdot 10^{-3}$	334.47
EVA	27.75	4994.05	$5.4 \cdot 10^{-5}$	$2.6 \cdot 10^{-3}$	349.93
SH	43.30	616.84	$1.3 \cdot 10^{-4}$	$4.3 \cdot 10^{-3}$	165.72

Finally, the corresponding pressure drops have been calculated (Table 7); these occur mostly in the superheater sections where the fluids are both gaseous and have higher velocities; overall, however, the values remain limited.

Table 7. *Pressure drops.*

Δp_{GAS}	Δp_{NH_3}
mbar	mbar
41	80

4.1 Energy balance

Subsequently, a comprehensive thermodynamic analysis of the entire process has been carried out, considering that the gaseous ammonia stream still passes through a reactor for cracking reaction, followed by a hydrogen separation stage through a membrane. Under current pressure and temperature conditions, the achievable conversion rate is around 72%; complete conversion is not reached because high pressures hinder the ammonia decomposition, as the reaction involves an increase in the number of moles from reactants to products. Therefore, additional heat must be supplied to raise the temperature to 700°C via a heater and achieve nearly complete conversion, in addition to the enthalpy required for the endothermic cracking reaction. Under these conditions, the total additional heat flow accounts for 12 MW. When combined with the thermal requirement of the upstream unit, the total demand reaches around 17 MW. However, by recovering waste heat from the exhaust gases for the heating and vaporisation phase in the thermal unit, the overall thermal demand can be reduced by approximately 31%. This represents a significant improvement in overall process efficiency and a substantial reduction in the consumption.

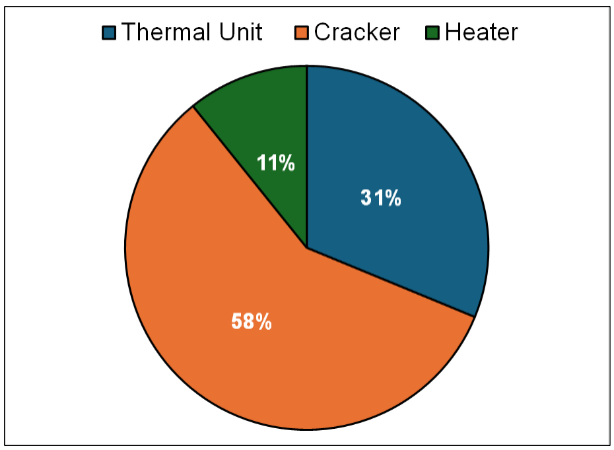

Figure 5. *Thermal consumption breakdown.*

Moreover, the possibility of burning the tail gas from the separation process has also been evaluated. This gas can be combusted; however, due to the high nitrogen content, its heating value is very limited (1.79 MJ/kg) to

sustain the reactor independently. Nevertheless, its combustion can still provide a meaningful contribution, covering approximately 28% of the external additional thermal power requirements.

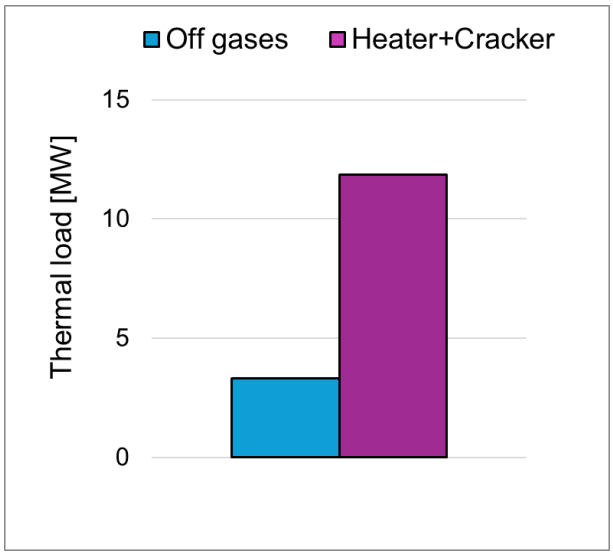

Figure 6. *Comparison between the thermal demand required by the heater and cracker components and the thermal power supplied by the off-gases combustion.*

In conclusion, when considering the heat recovered from the turbine exhausts during the heating and evaporation of ammonia, along with the heat recovered from the combustion of the off-gas in the subsequent stage, the result is a reduction of approximately 50% in global energy requirements.

4.2 Off-design analysis

To better understand the system's behaviour and its ability to adapt to variations in operating conditions in a real plant, the system response has been analysed by varying the gas turbine load, with the geometry fixed. As the turbine load varies, the inlet operating parameters change accordingly, particularly in terms of the exhaust-gas temperature and mass flow rate, thereby affecting the available thermal energy input. At reduced loads, the ammonia mass flow rate decreases, while the available energy per unit mass of the flow increases up to 19%. Therefore, reducing the mass flow rate while increasing the specific heat flux leads to a rise in the fluid's outlet temperature. For example, when the turbine operates at 40% of its nominal load, the ammonia outlet temperature can be approximately 26% higher than under the reference operating conditions (Figure 7).

Table 8. *Main input data as a function of load.*

Load	Q_{GAS}	m_{NH3}	$m_{NH3,tube}$
%	MW	kg/s	kg/s
100	28	2.26	0.038
80	24	1.92	0.031
60	22	1.62	0.027
40	19	1.20	0.020

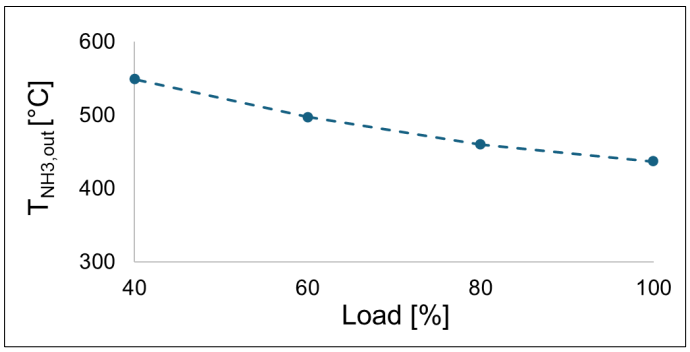

Figure 7*. Ammonia outlet temperature as a function of GT load.*

Moreover, if the mass flow rate decreases, the head losses in the pipe also decrease, following roughly a quadratic trend because the fluid speed reduces, which in turn lowers the friction against the walls of the pipe. This results in a reduction of 55% and 70%, respectively, for the gas and ammonia sides.

4.3 Energy balance

The same thermodynamic analysis has been carried out while varying the GT load. The parameters that have the greatest impact and determine the reduction in energy consumption are the lower required flow rate, as well as the reduced heat needed to reach 700 °C in the heating phase, since the outlet fluid is already at a higher temperature. Under 40% load conditions, a maximum reduction of 38% is achieved with the waste heat recovery in the thermal unit.

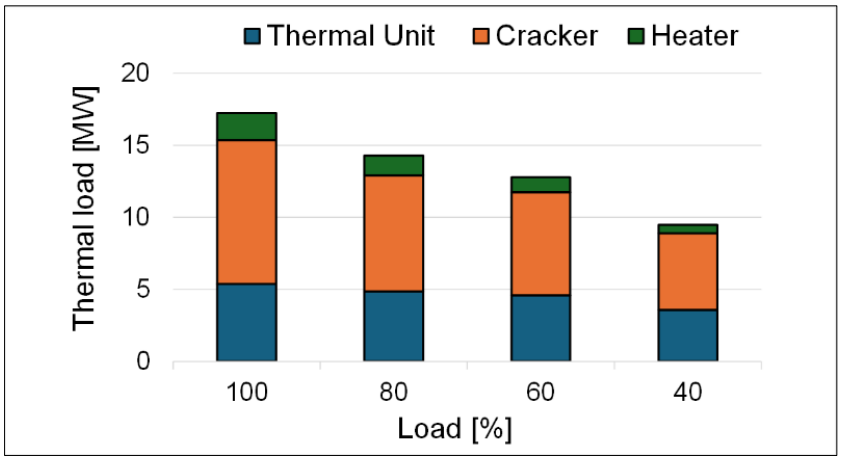

Figure 8. *Thermal consumption breakdown as a function of the GT load.*

In this case as well, the possibility of off-gas combustion has been evaluated as an additional strategy for thermal recovery within the process. On one hand, the external thermal energy required to sustain both the preheating phase and the endothermic ammonia cracking reaction is reduced, as aforementioned. On the other hand, the amount of recoverable heat available in the off-gas stream is also reduced. Despite this trade-off, the overall impact remains beneficial with an overall reduction of approximately 30% in the external thermal input required by the system. When this contribution is considered together with other heat recovery strategies implemented in the first phase, total energy savings can reach up to 56%.

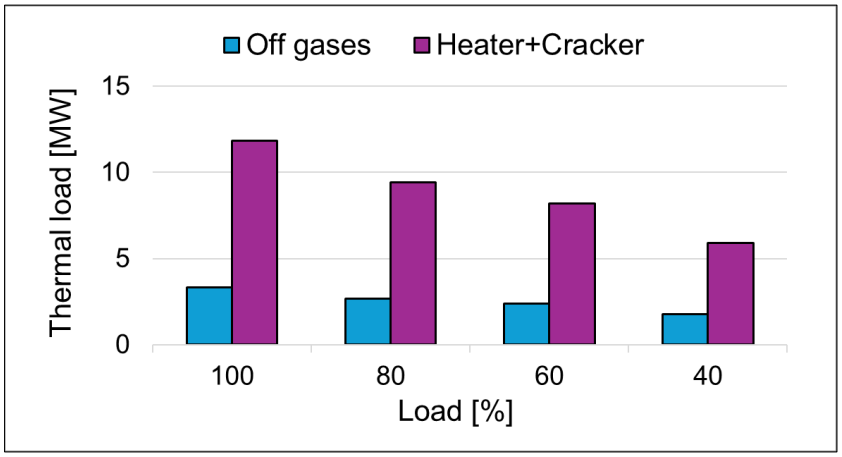

Figure 9. *Comparison between the thermal demand required by the heater and cracker components and the thermal power supplied by the off-gases combustion.*

5. Conclusions

The present study aims to develop a MATLAB-based model of a thermal unit, responsible for bringing ammonia from a liquid state to a high-temperature gaseous phase, required for the subsequent decomposition phase in a dedicated cracking reactor. Then, hydrogen is separated from the gas mixture and used as a fuel in the gas turbine. The adopted geometry is that of a cross-flow once-through unit with finned tubes and segmented finning. This design choice has been driven by the need to maximise the heat transfer area within a limited space. The developed approach allows the simulation of the thermal behaviour of the fluids as the system

geometry varies, using the ε-NTU method. Particular attention has been paid to the evaporation stage in which two phases coexist. Through this analysis, a configuration has been identified that enables the system to operate at 45 bar with an ammonia mass flow rate of 2.26 kg/s. The system is characterised by a frontal area of 18 m², internal tube diameters of 10 mm for the economiser and 25 mm for both the evaporator and the superheater, and the overall external tube diameter, including fins, is 40 mm. The larger diameter adopted in the evaporation and superheating sections is intended to prevent excessive fluid velocities, which result from the significant increase in the specific volume of ammonia. Under these operating conditions, the ammonia outlet temperature is 437°C. Subsequently, a comprehensive energy analysis of the system has been carried out, also taking into account the cracking reaction, for which additional external heat is required. Based on the overall energy balance, the introduction of the thermal unit results in an advantageous outcome, enabling a 31% reduction in thermal load through the recovery of heat from the flue gases. Moreover, the possibility of burning the tail gas produced during hydrogen separation has been considered, but due to its low lower heating value, only 28% of the required external heat can be supplied in this way. Overall, by using both strategies, an energy saving of 50% is achieved. Finally, analysis of variations in the gas turbine load revealed that at reduced load, better results in terms of outlet temperature can be achieved due to the lower mass flow rate and the higher available heat per unit of mass. Under 40% GT load conditions, the ammonia reaches a maximum temperature of 549 °C. The energy analysis shows that thanks to the recovery of waste heat, the thermal load is reduced up to 38%. Due to the lower mass flow rate and the higher outlet temperature from the superheater, when heat recovery through the combustion of tail gas is also taken into account, the total savings reach a maximum of 56%. In conclusion, the work conducted presents a model for recovering exhaust gases' heat, to vaporise and heat the ammonia for the subsequent cracking stage; nevertheless, the proposed system improves energy efficiency through the recovery of waste heat. Therefore, this model can also be effectively integrated in combination with other technologies where exhaust heat could be recovered.

Nomenclature

Bo	Boiling number
C_p	specific heat, J/(kg K)
C	heat capacity rate, W/K
Co	Convection number
D	diameter, m
ε	effectiveness
ECO	Economiser
EVA	Evaporator
f	Darcy friction factor
Fr	Froude number
G	mass flux, kg/(m^{2}s)
GHG	Greenhouse Gases
GT	Gas Turbine
h	heat transfer coefficient, W/(m^{2}K)
j	Colbrun factor
k	thermal conductivity, W/(mK)
N_{tr}	number of tubes per row
NTU	Number of Transfer Units
Nu	Nusselt number
Pr	Prandtl number
Q''	heat flux, W/m^2
r	ratio between the minimum and maximum heat capacity rate
Re	Reynolds number
SH	Superheater
St	Stanton number
T	Temperature, °C
U	overall heat transfer coefficient, W/(m^{2}K)

References

[1] Hannah Ritchie, Pablo Rosado, and Max Roser, "Greenhouse gas emissions - Our World in Data," *Our World in Data*, 2020, Accessed: Jan. 19, 2026. [Online]. Available: https://archive.ourworldindata.org/20260116-144923/greenhouse-gas-emissions.html

[2] A. Valera-Medina *et al.*, "Review on Ammonia as a Potential Fuel: From Synthesis to Economics," *Energy & Fuels*, vol. 35, no. 9, pp. 6964–7029, May 2021, doi: 10.1021/acs.energyfuels.0c03685.

[3] C. Willich, "Hydrogen as an Energy Carrier—An Overview over Technology, Status, and Challenges in Germany," *J (Basel).*, vol. 7, no. 4, pp. 546–570, Dec. 2024, doi: 10.3390/j7040033.

[4] N. Zhu, F. Yang, Y. Hong, and J. Liang, "Hydrogen production from ammonia decomposition: Advances in Ru- and Ni-based catalysts," Jan. 13, 2025, *Elsevier Ltd*. doi: 10.1016/j.ijhydene.2024.12.136.

[5] E. Spatolisano, L. A. Pellegrini, A. R. de Angelis, S. Cattaneo, and E. Roccaro, "Ammonia as a Carbon-Free Energy Carrier: NH3 Cracking to H2," *Ind. Eng. Chem. Res.*, vol. 62, no. 28, pp. 10813–10827, Jul. 2023, doi: 10.1021/acs.iecr.3c01419.

[6] S. Peters, A. M. Abdel-Mageed, and S. Wohlrab, "Thermocatalytic Ammonia Decomposition – Status and Current Research Demands for a Carbon-Free Hydrogen Fuel Technology," *ChemCatChem*, vol. 15, no. 2, Jan. 2023, doi: 10.1002/cctc.202201185.

[7] M. Aziz, F. B. Juangsa, A. R. Irhamna, A. R. Irsyad, H. Hariana, and A. Darmawan, “Ammonia utilization technology for thermal power generation: A review,” *Journal of the Energy Institute*, vol. 111, p. 101365, Dec. 2023, doi: 10.1016/j.joei.2023.101365.

[8] R. Ao, R. Lu, G. Leng, Y. Zhu, F. Yan, and Q. Yu, “A Review on Numerical Simulation of Hydrogen Production from Ammonia Decomposition,” Jan. 01, 2023, *MDPI*. doi: 10.3390/en16020921.

[9] P. Saini, D. Jampaiah, S. Periasamy, A. P. Kulkarni, and S. K. Bhargava, “Advances in ammonia decomposition catalysis: a comprehensive analysis of nanoparticle, single-atom, and metal cluster catalysts,” Mar. 14, 2025, *Royal Society of Chemistry*. doi: 10.1039/d5cc00953g.

[10] M. Asif *et al.*, “Recent advances in green hydrogen production, storage and commercial-scale use via catalytic ammonia cracking,” *Chemical Engineering Journal*, vol. 473, p. 145381, Oct. 2023, doi: 10.1016/j.cej.2023.145381.

[11] D. Pashchenko, R. Mustafin, and I. Karpilov, “Ammonia-fired chemically recuperated gas turbine: Thermodynamic analysis of cycle and recuperation system,” *Energy*, vol. 252, Aug. 2022, doi: 10.1016/j.energy.2022.124081.

[12] C. Romano *et al.*, “Ammonia Cracking As Auxiliary System for Gas Turbine: Preliminary Studies,” in *ASME 2024 Power Conference*, American Society of Mechanical Engineers, Sep. 2024. doi: 10.1115/POWER2024-137878.

[13] Z. Su *et al.*, “Research progress of ruthenium-based catalysts for hydrogen production from ammonia decomposition,” Jan. 02, 2024, *Elsevier Ltd*. doi: 10.1016/j.ijhydene.2023.09.107.

[14] D. Bellotti, C. Monacchini, C. Anfosso, C. Romano, E. Pucci, and L. Magistri, “Techno-Economic Assessment Of An Ammonia-Based Gas Turbine,” *J. Eng. Gas Turbine. Power*, pp. 1–17, Jan. 2026, doi: 10.1115/1.4070812.

[15] R. M. Combs, “WASTE HEAT RECOVERY UNIT DESIGN FOR GAS TURBINE PROPULSION SYSTEMS,” 1979.

[16] R. K. Shah and D. P. Sekulic, *FUNDAMENTALS OF HEAT EXCHANGER DESIGN*. John Wiley & Sons., 2003.

[17] F. P. Incropera, DeWitt D.P., Bergman T.L, and A. S. Lavine, *Fundamentals of heat and mass transfer (7th ed.)*. New York, NY: John Wiley and Sons., 2011.

[18] K. Silaipillayarputhur and S. Idem, “A general matrix approach to model steady-state performance of cross-flow heat exchangers,” *Heat Transfer Engineering*, vol. 34, no. 4, pp. 338–348, Jan. 2013, doi: 10.1080/01457632.2013.716347.

[19] S. G. Kandlikar, “A General Correlation for Saturated Two-Phase Flow Boiling Heat Transfer Inside Horizontal and Vertical Tubes,” 1990. [Online]. Available: http://asmedigitalcollection.asme.org/heattransfer/article-pdf/112/1/219/5644274/219_1.pdf

[20] S. G. Kandlikar and P. Balasubramanian, “An Extension of the Flow Boiling Correlation to Transition, Laminar, and Deep Laminar Flows and Microchannels,” in *Heat Transfer Engineering*, Apr. 2004, pp. 86–93. doi: 10.1080/01457630490280425.

[21] F. Faraji, C. Santim, P. L. Chong, and F. Hamad, “Two-phase flow pressure drop modelling in horizontal pipes with different diameters,” *Nuclear Engineering and Design*, vol. 395, Aug. 2022, doi: 10.1016/j.nucengdes.2022.111863.

[22] “Compatibility table.” Accessed: Jan. 20, 2026. [Online]. Available: https://www.metalwork.it/media/Stumenti_manuali/Tab_compatibilita.pdf